Recent Results of the TierPET Scanner

S. Weber, A. Bauer*, H. Herzog*, F. Kehren*, H. Mühlensiepen*, J. Vogelbruch, H. H. Coenen+, K. Zilles*, H. Halling

Zentrallabor für Elektronik, *Institut für Medizin, +Institut für Nuklearchemie,
Forschungszentrum Jülich, 52425 Jülich, Germany

Abstract

At the Forschungszentrum Jülich a high resolution positron emission tomograph (TierPET) for imaging small laboratory animals, especially rats, has been constructed. The scanner is based on arrays of YAP crystals. As a special feature the detector distances can be varied continuously from 16 to 58 cm. Due to the variable detector distances the performance of the scanner has to be evaluated in various configurations. Special attention was paid to dedicated data acquisition protocols and adequate applications with regard to the system sensitivity.

I. INTRODUCTION

High resolution positron emission tomography is an important tool for studying *in vivo* tracer pharmacokinetics and metabolism. It may play a promising role in drug development and studies of human diseases using animal models. At present, *in vitro* receptor autoradiography is widely used to investigate those topics. This technique, however, does not allow repeated studies within the same animal and it is difficult to investigate dynamic processes which may occur after experimental intervention. High resolution PET with a spatial resolution of about 2 mm may help to get access to these experimental conditions.

The conditions for small animal scans, especially the small size of the required field-of-view, allow a reduction of the amount of detectors compared to human scanners and thus more flexibility in detector design which is reflected in various scanner designs [1-9]. The tomograph described here uses matrices of Yttrium Aluminium Perovskit (YAP) crystals, and a special feature is the possibility to change the detector distances. The performance of the scanner may be different for various center-detector distances which means that performance measurements have to be performed for several distances. We focus particularly on the scanner characterization for various center-detector distances as well as dedicated data acquisition protocols which benefit from the variable detector distances.

II. THE TIERPET SCANNER

A complete description of the TierPET scanner including important design characteristics as well as a performance evaluation has been reported previously [10]. The primary characteristics of the scanner are listed in Table I. A TierPET detector consists of a 20 by 20 array of individual 2 x 2 x 15 mm Yttrium Aluminum Perovskit (YAP) crystals which are polished and optically isolated by thin reflective layers. The arrays are coupled to a Hamamatsu R2487 position sensitive PMT. The four planar detectors can be placed at various radial positions ranging from 8 to 29 cm. The scanner acquires data exclusively in 3D mode. The data are taken in list mode and are presently converted into 2D sinograms using a multiple slice rebinning method [11].

Table I
Main characteristics of the TierPET scanner

Detector	
Number of detectors	4
Scintillator material	Yttrium Aluminum Perovskit (YAP)
Crystal size	2 x 2 x 15 mm^3
Number of crystals	20 x 20 crystals per module
Photomultiplier	Hamamatsu R2487
Geometry	
Detector-detector distance	variable, 16 to 58 cm
Axial FOV	40 mm
Transaxial FOV	40 mm diameter
Data	
Data acquisition	3D, step and shoot, List mode
Reconstruction	2D, ML-EM, Multiple Slice Rebinning

III. PERFORMANCE MEASUREMENTS

A. Spatial resolution

The spatial resolution of the system was measured using a [^{18}F]-FDG filled needle of 0.9 mm diameter placed in air at the center of the field of view and at 4, 8, 12 and 16 mm off-center. The scans were performed for center-detector distances of 100, 140, 160, 180, 200 and 240 mm. The FWHM was obtained after reconstruction from the line profiles using linear interpolation. The measured and the line source profiles were

0018-9499/00$10.00

deconvolved to correct for the line source width. It was shown before [10] that the resolution is homogeneous over the field of view, so the resolution values can be averaged over the field of view.

B. Scatter fraction

The scatter fraction was measured using a 6 cm diameter, 6 cm high water filled phantom. A [^{18}F]-FDG filled line source was positioned at the center of the phantom and at radial positions of 7 and 14 mm. Center-detector distances were 100, 140, 160, 180 and 200 mm. After conversion of the list mode data into sinograms the sinogram profiles were used to calculate the scatter fraction. The sinograms were treated following the method proposed in [12]. For each projection angle and for 7 central slices the pixel with the largest value was found and the projection was shifted so that the pixel containing the maximum value was aligned with the central pixel of the sinogram. All projections were summed, and a polynomial function was fitted to the wings of the profile and extrapolated under the central peak. The total and scattered counts for the 3 positions in the FOV were decay corrected and weighted by the area of the annulus at the respective radial position. The scatter fraction was then calculated as the ratio of scattered and total counts.

C. Noise equivalent counts

Noise equivalent count rate performance was measured using a 100 ml ^{11}C filled phantom ($t_{1/2}$=20.4 min) for center-detector distances of 100, 140, 180 and 200 mm. The phantom was scanned over 9 isotope half-lives. Random coincidences were measured using the delayed coincidence method. The width of the coincidence window is 250 ns. Total and random counts were collected in turn every 1.5 min without dynamic discrimination [10]. The noise equivalent count rates (NEC) have been calculated from the measured totals and random counts following [13].

D. Sensitivity Profile

The TierPET system uses two pairs of planar detectors. Each detector is solely in coincidence with its opposite detector. Due to the geometry the sensitivity of the scanner shows a strong variation over the field of view which has to be corrected during data preprocessing. Events in the center of the field of view are detected with highest probability whereas annihilation photons from the edge of the field of view mostly hit only one of the coincident detectors and miss the other one for geometrical reasons.

The sensitivity profile has been measured for a center-detector distance of 280 mm. A ^{68}Ge point source was moved over the field of view in steps of about 1 cm, and the count rate was measured and deadtime corrected.

E. Dedicated Data Acquisition for Sensitivity Enhancement

Due to the low Z of the YAP crystals and the small detector areas the sensitivity of the TierPET is relatively low. In order to overcome this disadvantage, a dedicated data acquisition method has been developed. Detector distances are reduced within successive time frames to keep the count rate near the maximum of the NEC curve for the whole data acquisition and to compensate for the radioactive decay or biological washout of the radiopharmaceutical.

The conditions for a reconstruction without distortion for the variable detector distance data sets are well adapted corrections, especially detector normalization, for each of the detector distances, during data preprocessing. Detector normalization is performed by normalizing the single detectors and calculating the sensitivity of the LOR's during conversion of the variable detector distance list mode data into sinograms. For a demonstration of the feasibility of this kind of data acquisition a 10 ml injection syringe was filled with 100 µCi of [^{18}F]-FDG and scanned with center-detector distances of subsequently 200 (2 time frames), 180 (2), 160 (4), 140 (10) and 100 mm (10). After reconstruction the ROI average of the homogeneous activity distribution was calculated for each time frame.

IV. Results

A. Spatial resolution

Figure 1 shows the spatial resolution for the 6 center-detector distances, averaged over the 5 positions in the field of view. There is hardly a variation in spatial resolution for the detector distances which are used for animal scans. Simulation results have shown [14] that the resolution deteriorates for center-detector distances below 80 mm, but for practical reasons (detector housing, width of rat bed, fixation of the rat, etc.) these small distances are not used. For source-detector distances of 100 to 200 mm the FWHM is within the error bars, and the spatial resolution is about 2.1 mm. Deterioration of spatial resolution due to annihilation photon non-collinearity begins for a center-detector distance above 240 mm. As a result, the variation of the detector distances can be used in practice to adapt the system to the available count rate regardless of the variation in spatial resolution.

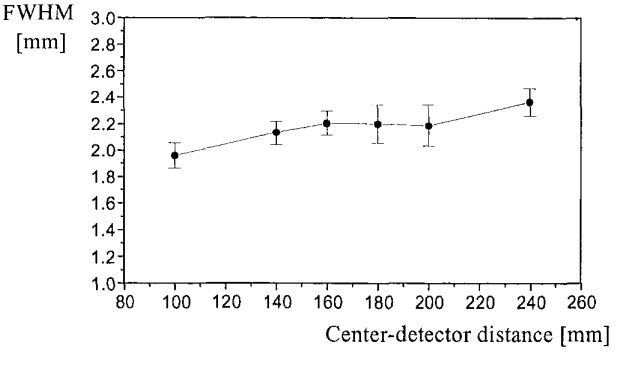

Figure 1: Spatial resolution of the TierPET for various source-detector distances.

B. Scatter fraction

The scatter fraction was determined for dynamic discriminator levels [10] of 200 keV and 350 keV. Table 2 shows the respective scatter fractions. The scatter fraction is low due to

the geometry of the scanner. Often the scattered events will miss one of the detectors.

Table 2
Scatter fraction

Center-detector distance	200 keV	350 keV
100 mm	15.4 %	13.4 %
140 mm	15.2 %	11.3 %
160 mm	11.9 %	10.6 %
180 mm	12.2 %	9.4 %
200 mm	13.9 %	9.3 %

C. Noise equivalent counts

The noise equivalent count rate performance of the TierPET system is displayed in Figure 2 for 4 different center-detector distances. NEC maximum amounts to 592 cps (100 mm), 563 cps (140 mm), 553 cps (180 mm) and 492 cps (200 mm).

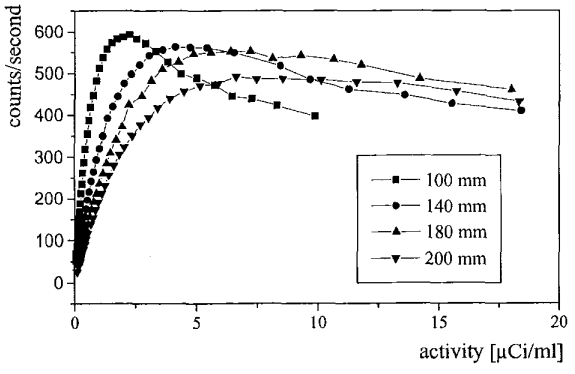

Figure 2: Noise equivalent count rate performance; center-detector distances are 100, 140, 180 and 200 mm respectively.

D. Sensitivity Profile

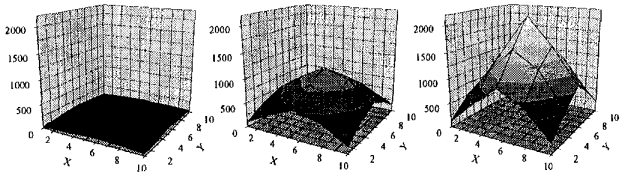

(a) (b) (c)

Figure 3: Sensitivity profile for different axial positions:
(a) beginning of the axial field of view; (b) between edge and center of the axial field of view; (c) center of the axial field of view.

Figure 3 shows the x-y-sensitivity profile of the scanner for 5 different axial positions. Figure 3(a) shows the sensitivity profile at the beginning of the axial field or view, figure 3(b) the plane between the center and the beginning of the field of view and figure 3(c) the plane directly at the center. The scanner is most sensitive at the center of the field of view, the sensitivity at the edges drops to 1.5 % of the maximum. This behaviour leads to large geometrical correction factors for the less sensitive areas and limits the useful field of view to about 2 cm in diameter.

E. Dedicated Data Acquisition for Sensitivity Enhancement

Figure 4(a) shows the count rate throughout the scan of the homogeneously filled injection syringe. The acquired count rate is displayed on the top, the expected count rate without change of detector distance on the bottom. Figure 4(b) shows the decay corrected average of a region of interest of the activity distribution. The ROI average is constant within the error bars, so that it could be shown that the variable detector distance data acquisition is suitable to increase the system sensitivity. This method is of special interest for scans with short living radioisotopes containing for example ^{11}C.

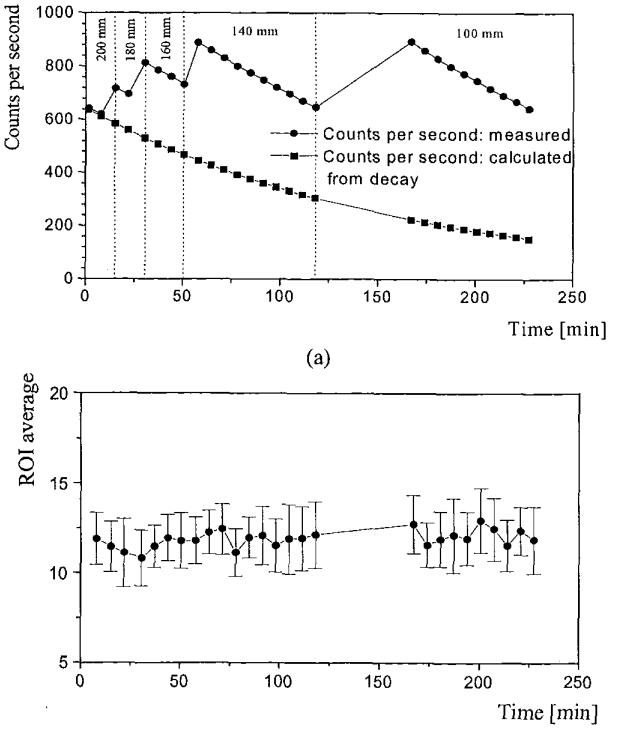

Figure 4: (a) Counts per second measured and calculated from radioactive decay, (b) decay corrected ROI average for a homogeneous activity distribution of [^{18}F]-FDG scanned with variable detector distances.

V. Applications: In-Vivo Measurements

The feasibility of the TierPET for *in vivo* measurements was assessed by investigating some typical applications for a high resolution PET.

A. Rat Brain [^{18}F]-FDG Uptake

After feed restrictance over night a Sprague Dawley rat was short-time anesthetised to inject [^{18}F]-FDG. The rat was allowed to wake up for 30 minutes in order to enhance brain metabolism and was consecutively anesthetised for the PET scan. Total scan time was 79 minutes, total number of counts were $4.3*10^6$. After the scan the rat was sacrificed and the

brain was removed. Two hours after injection the brain was scanned with the TierPET for again 79 minutes. Total number of counts were $2.8*10^6$. Figure 5 shows two slices of the living brain and one slice of the dissected brain. There is a massive tracer uptake within the Harderian glands, which are extracranially located within the orbit. The signal of the Harderian glands is shown in Figure 5(a). FDG uptake in the living brain is given in Figure 5(b) which shows also an uptake in extracranial tissue. A coronal section of the removed brain is given in figure 5(c).

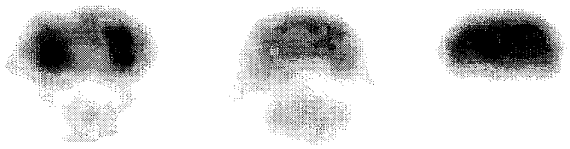

(a) (b) (c)

Figure 5: [^{18}F]-FDG uptake in coronal sections of a rat cranium. (a) Harderian glands; (b) brain in situ; (c) removed brain.

B. Rat Brain [^{18}F]-N-methyl-benperidol Uptake

The dopamine D2 neuroreceptor ligand [^{18}F]-N-methyl-benperidol [15] exhibits a high binding capacity in the striatum. Additionally there is a high uptake of the ligand in the Harderian glands.

A Sprague Dawley rat was injected with 2 mCi [^{18}F]-N-methyl-benperidol and scanned for 60 minutes. Total number of counts were $3.7*10^6$. After the scan the head of the rat was cut into slices and an autoradiography of the complete head was performed. Figure 6 (a) shows the distribution of the receptor ligand in the striatum and the Harderian glands measured with autoradiography. Figure 6(b) shows the same region in the TierPET scan. The striatum can be clearly separated from the Harderian glands even in the TierPET scan due to the high volumetric resolution of the TierPET.

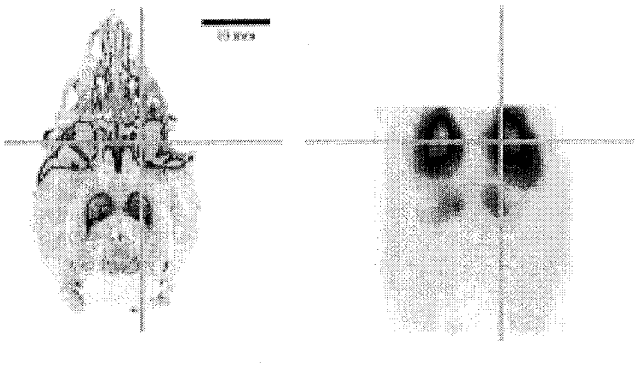

(a) (b)

Figure 6: Transversal sections of [^{18}F]-N-methyl-benperidol uptake in a rat brain and Harderian glands: (a) autoradiography and (b) TierPET.

VI. Conclusions

The main advantage of the presented scanner is its flexibility. The special feature of the TierPET, the variable detector distances, required an evaluation of the performance characteristics for various configurations. The spatial resolution shows hardly a variation with the detector distances which are used in practice. The trade-off between resolution and sensitivity appears to be weak concerning the resolution in this region, pointing to choose detector distances as short as possible. A dedicated data acquisition method for this type of scanner is, therefore, a decrease of detector distances between two time frames which requires well adapted correction methods.

Due to the variations in the sensitivity over the field of view the measurement of a widespread activity distribution such as FDG studies in the rat brain is not an ideal application for the TierPET. Imaging low-contrast, extended objects like the FDG distribution in the brain requires considerably more counts than high-contrast, point-like structures. In case of the rat brain, the problem is compounded by the fact that most of the FDG goes to extracranial sites like the Harderian glands. This activity produces excess noise in the brain volume-of-interest, so that even more counts are necessary to achieve good image quality. The pyramidal nature of the sensitivity leads to a larger number of counts from the center of the field-of-view whereas the regions outside of the center suffer from a lower countrate, which means that large correction factors have to be applied to compensate for the variation in sensitivity. The current data acquisition system with a NEC maximum around 600 cps does not allow to acquire sufficient counts from the whole field-of-view for a good quality FDG brain image.

Adequate applications are measurements of concentrated activity distributions in the central 2 cm of the field of view, for example receptor binding studies looking at the striatum of the rat.

VII. Acknowledgements

We would like to thank Chandra Patel for carrying out the performance measurements. The images are displayed using the MPI tool, developed by the Max-Planck-Institute for Neurological Research, Cologne, Germany.

VIII. References

[1] P. M. Bloomfield, R. Myers, S. P. Hume, T. J. Spinks, A. A. Lammertsma, T. Jones, "Three dimensional performance of a small-diameter positron emission tomograph," *Phys. Med. Biol.*, vol. 42, p. 389, 1997.

[2] P. Bruyndonckx, X. Liu, S. Tavernier, S. Zhang, "Performance study of a 3D small animal PET scanner based on BaF_2 crystals and a photo sensitive wire chamber," *Nucl. Instrum. and Meth. A,* vol. 392, p. 407, 1997.

[3] S. R. Cherry, Y. Shao, R. W. Silverman, K. Meadors, S. Siegel, A. Chatziioannou, J. W. Young, W. F. Jones, J. C. Moyers, D. Newport, A. Boutefnouchet, T. H. Farquhar, M. Andreaco, M. J. Paulus, D. M. Binkley, R. Nutt, M. E. Phelps, "MicroPET: A high resolution PET scanner for imaging small animals," *IEEE Trans. Nucl. Sci.,* vol. 44, no. 3, p. 1161, 1997.

[4] R. Lecomte, J. Cadorette, S. Rodrigue, D. Lapointe, D. Rouleau, M. Bentourkia, R. Yao, P. Msaki, "Initial results from the Sherbrooke avalanche photodiode positron tomograph," *IEEE Trans. Nucl. Sci.*, vol. 43, no. 3, p. 1952, 1996.

[5] M. Watanabe, H. Okada, K. Shimizu, T. Omura, E. Yoshikawa, T. Kosugi, S. Mori, T. Yamashita, "A high resolution animal PET scanner using compact PS-PMT detectors," *IEEE Trans. Nucl. Sci.*, vol. 44, no. 3, p. 1277, 1997.

[6] W. W. Moses, P. R. G. Virador, S. E. Derenzo, R. H. Huesman, T. F. Budinger, "Design of a high-resolution, high-sensitivity PET camera for human brains and small animals," *IEEE Trans. Nucl. Sci.*, vol. 44, no. 4, p. 1487, 1997.

[7] J. L. Robar, C. J. Thompson, K. Murthy, R. Clancy, A. M. Bergman, "Construction and calibration of detectors for high-resolution metabolic breast cancer imaging," *Nucl. Instrum. and Meth. A*, vol. 392, no. 1-3, p. 402, 1997.

[8] A. del Guerra, F. de Notaristefani, G. di Domenico, M. Giganti, R. Pani, A. Piffanelli, A. Turra, G. Zavattini, "Use of a YAP:Ce matrix coupled to a position-sensitive photomultiplier for high resolution positron emission tomography," *IEEE Trans. Nucl. Sci.*, vol. 43, no. 3, p. 1958, 1996.

[9] O. Fries, S. M. Bradbury, J. Gebauer, I. Holl, E. Lorenz, D. Renker, S. Ziegler, "A small animal PET prototype based on LSO crystals read out by avalanche photodiodes," *Nucl. Instrum. and Meth. A*, vol. 387, p. 220, 1997.

[10] S. Weber, H. Herzog, M. Cremer, R. Engels, K. Hamacher, F. Kehren, H. Mühlensiepen, L. Ploux, R. Reinartz, P. Reinhart, F. Rongen, F. Sonnenberg, H. H. Coenen, H. Halling, "Evaluation of the TierPET scanner", *IEEE Trans. Nucl. Sci.*, vol. 46, no. 4, p. 1177, 1999

[11] R. M. Lewitt, G. Mühllehner, J. S. Karp, "Three-dimensional image reconstruction for PET by multiple slice rebinning and axial image filtering," *Phys. Med. Biol.*, vol. 39, pp. 321-339, 1994

[12] NEMA Standards Publication NU 2-1994, "Performance measurements of positron emission tomographs", National Electrical Manufacturers Association, 2101 L. Street, NW, Washington, DC 20037-1526

[13] S. C. Strother, M. E. Casey, and E. J. Hoffman, "Measuring PET scanner sensitivity: relating countrates to image signal to noise ratios using noise equivalent counts," *IEEE Trans. Nucl. Sci.*, vol. 37, no. 2, p. 783, 1990

[14] S. Weber, A. Terstegge, H. Herzog, R. Reinartz, P. Reinhart, F. Rongen, H. W. Müller-Gärtner, H. Halling, "The design of an animal PET: Flexible geometry for achieving optimal spatial resolution or high sensitivity", *IEEE Trans. Med. Imaging*, vol. 16, no. 5, p. 684, 1997

[15] K. Hamacher, W. Hamkens, "Remote controlled one-step production of [^{18}F] labeled butyrophenone neuroleptics exemplified by the synthesis of n.c.a. [^{18}F] N-methylspiperone," *Appl. Radiat. Isot.*, vol. 46, no. 9, p. 911, 1995